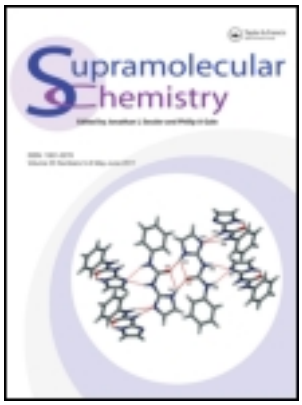

Supramolecular Chemistry
Publication details, including instructions for authors and subscription information:
http://www.tandfonline.com/loi/gsch20

pH tunable self-assembly of chicoric acid and their biocompatibility studies

Evan M. Smoak [a], Karl R. Fath [b], Stacey N. Barnaby [a], Valerie C. Grant [a] & Ipsita A. Banerjee [a]

[a] Department of Chemistry, Fordham University, 441 E. Fordham Road, Bronx, NY, 10458, USA

[b] Department of Biology, Queens College, City University of New York and the Graduate Center, Kissena Boulevard, Flushing, NY, 11367, USA

Available online: 14 Sep 2011

To cite this article: Evan M. Smoak, Karl R. Fath, Stacey N. Barnaby, Valerie C. Grant & Ipsita A. Banerjee (2011): pH tunable self-assembly of chicoric acid and their biocompatibility studies, Supramolecular Chemistry, 23:10, 678-688

To link to this article: http://dx.doi.org/10.1080/10610278.2011.601309

Supramolecular Chemistry
Vol. 23, No. 10, October 2011, 678–688

pH tunable self-assembly of chicoric acid and their biocompatibility studies

Evan M. Smoak[a], Karl R. Fath[b], Stacey N. Barnaby[a], Valerie C. Grant[a] and Ipsita A. Banerjee[a]*

[a]*Department of Chemistry, Fordham University, 441 E. Fordham Road, Bronx, NY 10458, USA;* [b]*Department of Biology, Queens College, City University of New York and the Graduate Center, Kissena Boulevard, Flushing, NY 11367, USA*

(*Received 24 August 2010; final version received 4 June 2011*)

We report for the first time, the pH tunable self-assembly of chicoric acid, an HIV-I integrase inhibitor, which displayed a remarkable tendency to self-assemble at room temperature into varying nano- and microstructures. Furthermore, those assemblies were then functionalised with gold (Au) nanoparticles. We then investigated the biocompatibility of the materials by conducting *in vitro* cell attachment and cytotoxicity studies using normal rat kidney cells. The studies revealed that the biomaterials were non-toxic and biocompatible, and showed considerable adhesion to the cells. These results suggest that the assemblies could potentially be used for a variety of applications, such as carriers for targeted drug delivery as well as optoelectronics and sensors. Furthermore, the formation of highly organised nano- and microstructures of medicinally significant phytohormones such as chicoric acid is of particular interest as it might help in further understanding the supramolecular assembly mechanism of higher organised biological structures for the development of building blocks for various device fabrications.

Keywords: self-assembly; chicoric acid; gold nanoparticles; biocompatibility

Introduction

In recent years, molecular self-assembly processes of functionalised, supramolecular nano- and micro-architectures have acquired much attention because of the control they offer over the size and resultant morphology of the constructs (*1–3*). Largely due to non-covalent intermolecular and intramolecular interactions such as van der Waals forces, electrostatic interactions and hydrogen bonding, molecular self-assembly allows for the formation of varied supramolecular structures, whose morphology can be controlled by external factors such as pH, solvent system, temperature and concentrations (*4–9*). Thus, molecular self-assembly has become integral to the development of nanoscale devices for use in biomedicine, catalysis and biosensors (*10–13*). Self-assembly of biomolecules such as lipids, oligonucleotides, DNA, proteins and peptides have been investigated to create novel templates which has been designed to mimic channel proteins as well as to adhere drug molecules, adsorb proteins or conjugate with metallic and semiconductor nanoparticles (*14–19*). Recent studies have shown that when DNA is mixed with cationic liposomes, the resulting complexes form multilamellar structures consisting of alternating layers of DNA and lipid bilayers. These supramolecular structures have potential use as non-viral gene delivery vectors (*20*). Alternatively, research has also focused on the growth of hollow lipid tubes, which have been reported to have temperature-tunable diameter (*21*). Studies related to the self-assembly of synthetic organic materials have also been carried out. For example, highly fluorescent-conjugated pyridine (or pyrimidine) and cyano ligands have recently been synthesised. Furthermore, those compounds were reacted with rhenium complexes to form cyclic supramolecules by self-assembly processes (*22*). Such highly fluorescent molecules might find use in bioimaging or as sensors. In another study, molecular self-assembly of amphiphilic hyper-branched copolymers were found to produce long multi-walled tubes up to centimetres in length (*23*). Scientists have also reported the design and synthesis of peptide–polymer hybrids, which can self-assemble into stimuli-sensitive hydrogels (*24*). It has also been reported that inorganic compounds such as polyoxomolybdate-based molecules can self-assemble slowly over a period of months into vesicle-like structures in aqueous solutions (*25*).

Though several studies have been carried out to elucidate the self-assembly processes of synthetic organic/inorganic molecules as well as different types of biological assemblies, relatively less attention has been paid to the self-assembly of naturally occurring phytohormones. Many biomolecules found in nature, such as phytohormones, have interesting properties that may allow for their use as building blocks for the development of nanoscale devices. For example, the targeted delivery of phenolic caffeoyl derivatives such as those found in the *Echinacea* plant have been used to successfully inhibit the

*Corresponding author. Email: banerjee@fordham.edu

ISSN 1061-0278 print/ISSN 1029-0478 online

http://dx.doi.org/10.1080/10610278.2011.601309
http://www.tandfonline.com

active sites of the botulinum toxin (*26*). Other plant products such as artemisinins have been found to have antimalarial activity (*27*). With many plant species yet untapped in terms of potentially bioactive molecules, researchers have begun to investigate the potential applications of nature's bounty in both self-assembled architectures and their potential biomimetic or biological significance when conjugated with metal nanoparticles. Gibberellic acid, a plant cytokinin, for example, has been conjugated with amine moieties and was found to act as templates for the formation of gold nanoparticles. Further, gibberellic acid may also be used as immunotracers for several biological applications (*28*, *29*). In another study, *trans*-Zeatin has been shown to have the ability to selectively mineralise Au^{3+} ions on the surface of its self-assembled nanoarchitectures (*30*). Thus, self-assembled architectures of biomolecules obtained from naturally occurring phytohormones may allow for the creation of building blocks for the development of nanomaterials with enhanced abilities for various device fabrications from biosensors to electronics and optical devices (*31*).

To this end, silver nanoparticles have been conjugated to self-assembled systems of chitosan to enhance antibacterial effects (*32*). Furthermore, quantum dots, because of their high photoluminescence, have found use as bioimaging tools and advanced catalysts once conjugated to biomolecules or biomolecular architectures (*33*). Similarly, gold nanoparticles have been employed in bioimaging, drug delivery and electronic devices as well (*34–40*). Researchers have used gold nanoparticles in sensing infectious diseases by coupling the nanoparticles to fluorophores and antibodies, respectively (*41*). Additionally, thiocholine inhibition sensors were created by the enzyme-catalysed growth of gold nanoparticles on chitosan templates. These gold-conjugated templates were then used to immobilise acetylcholinesterase, which was utilised as an electrochemical sensor (*42*). In particular, many past works have shown that several fibrillar structures serve as attractive templates for attachment to metal nanoparticles and quantum dots (*43*). Furthermore, it was demonstrated that quantum dots could not only be incorporated into the fibrillar gels, but could also remain fluorescent. Other gelators have been explored separately, such as those based on bile acid (*43b*). Converting the carboxylic acid groups to a thiol, allowed for the gel to lock and stabilise metal nanoparticles. The attraction of thiol groups for metal nanoparticles has been extensively studied. For example, gold nanoparticles stabilised by a synthesised gelator containing two functional groups, a *trans*-1,2-bis(alkylamide)cyclohexane unit with two thiol groups (*43c*). Similarly, it has been shown that self-assembled pseudopeptide (cysteine containing C-terminally protected dipeptide) has the ability to stabilise both silver and gold nanoparticles (*43d*).

Recently, there has been increasing interest in chicoric acid, a compound found readily in *Echinacea purpurea* and common sweet basil, because of its activity as an HIV-I integrase inhibitor (*44*). While many phytochemicals such as dicaffeoylquinic acid and quinolinonyl diketo acids (*45*) have been found to have anti-HIV-I activity, chicoric acid, (dicaffeoyltartaric acid) is of particular interest because of its high degree of molecular symmetry and its dicarboxylic moieties which make it a fascinating molecule to explore for the development of assemblies for building blocks for device fabrications. In this work, we report the pH-tunable self-assembly of chicoric acid resulting in the formation of nano- and micro-assemblies depending on growth conditions. Furthermore, the self-assembled nanostructures were used as templates for binding gold nanoparticles for potential applications in bioimaging. The biocompatibility and cellular adhesion of the self-assembled chicoric acid assemblies as well as gold nanoparticle-coated assemblies were examined in the presence of normal rat kidney (NRK) epithelial cells. Such self-assembled nano- and microstructures might potentially display enhanced effectiveness as biosensors, agents for bioimaging or potential as drug delivery vectors to targeted cells.

Results and discussion

Self-assembly of chicoric acid

Typically, self-assembly is governed by non-covalent intermolecular forces, such as hydrogen bonding, van der Waals, forces and ionic interactions (*46*, *47*). The chemical structure of chicoric acid is shown in Figure 1. Because of the presence of the phenolic hydroxyl groups as well as dicarboxylic moieties, chicoric acid has the potential for a relatively high degree of both intramolecular and intermolecular interactions between the adjacent carboxylic groups and neighbouring keto-ester functionalities, as well as $\pi-\pi$ stacking interactions due to the phenol ring systems.

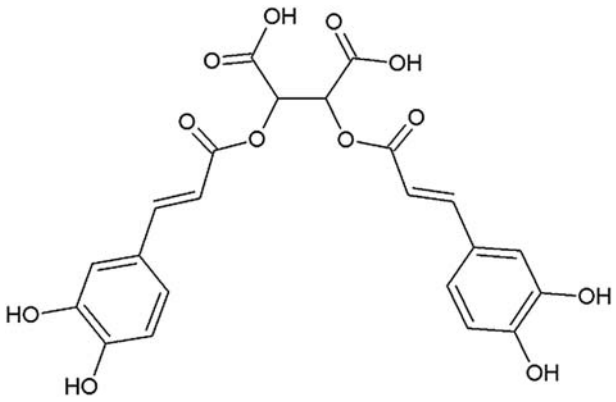

Figure 1. Chemical structure of chicoric acid.

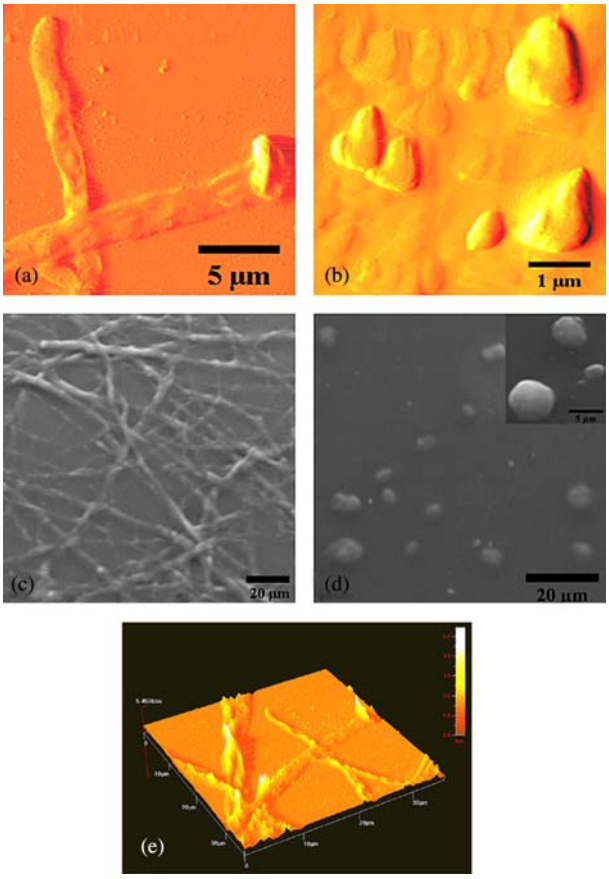

Figure 2. Amplitude AFM images of chicoric acid self-assembled at (a) pH 4 and (b) pH 8. SEM images of chicoric acid self-assembled structures at (c) pH 3 and (d) pH 8. Inset of (d) shows magnified image of microspheres grown at pH 8. (e) 3D AFM topography image of the microtubular assemblies formed at pH 3.

Due to the presence of specific functional groups, and the overall chemical structure of chicoric acid, we hypothesised that chicoric acid would most likely undergo self-assembly under aqueous conditions. Chicoric acid was self-assembled at a pH range of 3–10. After three to four weeks of self-assembly, the samples were analysed by AFM and SEM to investigate the surface details and the morphologies of the self-assembled architectures. The AFM images indicate that under acidic conditions ($\leq$ pH 5) (Figure 2(a)), dense networks of nanotubes and fibres ranging in diameter from 200 nm to 4 μm formed, whereas at relatively high pH ($\geq$ pH 8) (Figure 2(b)), globular architectures were observed. It is most likely that the presence of hydroxyl moieties of chicoric acid as well as high degree of protonation of the carboxyl groups under acidic conditions, lead to increased hydrogen bonding, lending to the formation of the highly branched structures at low pH. Stacking interactions between the aromatic polyphenolic ring systems may also be involved in stabilising the structures.

At higher pH, however, the carboxyl groups are deprotonated, and the proximity of the two carboxylic acid groups within the structure of chicoric acid may lead to subsequent electrostatic repulsion of the negatively charged carboxylate moieties. Thus, hydrogen bonding due to the carboxylate groups is also significantly reduced, inhibiting the formation of the types of larger structures formed at lower pH. However, the stacking interactions of the phenolic rings as well as the hydrogen-bonding ability between the hydroxyl groups still exist (pK_a of phenolic hydroxyl groups >8) (*48*) aiding in the formation of smaller fibrillar or spherical architectures. SEM images of chicoric acid assemblies at low pH (Figure 2(c)) and at high pH (Figure 2(d)) further confirmed the formation of these specific architectures. The fibrillar networks found at low pH contained branches exceeding 15 μm in length in some cases, whereas the microspheres seen at high pH were typically between 1 and 6 μm in diameter, as shown by AFM imaging. The three-dimensional (3D) AFM topography image (Figure 2(e)) shows the extensive networks of the fibrillar structures formed at pH 3.

At neutral pH ($\sim$ pH 7), the self-assembled architectures mostly showed a mixture of singular nano- and microtubular structures as well as spheres (Figure 3(a)). The spheres reached an average diameter of about 1 μm, whereas the tubular structures reached a diameter of about 200 nm–1 μm. This behaviour is expected, because the species is not completely deprotonated; hence, both types of structures are observed. However, under those conditions, the degree of protonation is significantly lesser than that observed at low pH.

It is plausible that such self-assembled morphologies formed under neutral conditions may also form *in vivo*. Proposed 3D models for the structures formed are shown in Figure 3. The dotted lines indicate hydrogen-bonding interactions. At low pH (Figure 4(a)), due to the presence of the —COOH groups, intermolecular and intramolecular

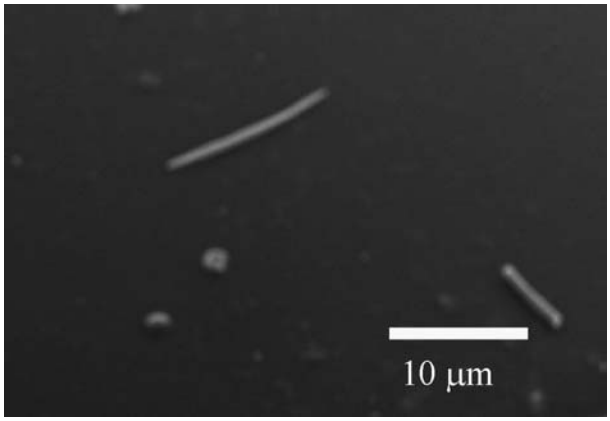

Figure 3. Self-assembled microtubules and microspheres formed at neutral pH.

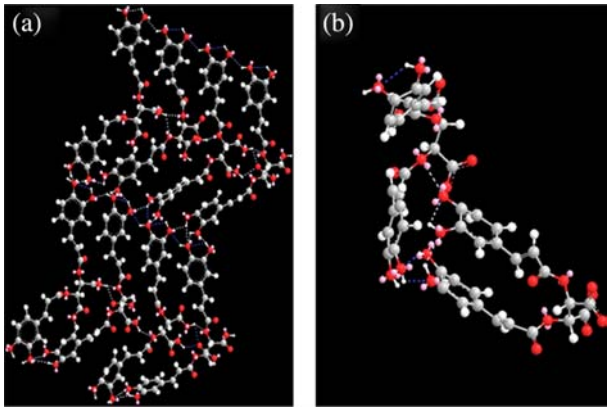

Figure 4. Proposed molecular model of the self-assembly of chicoric acid. (a) At pH <5 and (b) at pH >7.

interactions are observed between the carboxyl hydrogens and the C═O of the keto-ester groups. Furthermore, the phenolic hydroxyl groups also show both hydrogen-bonding and stacking interactions. Overall, it appears that the structures tend to fold up like sheets, similar to β-sheets in proteins, forming tubular, or fibrillar and ribbon-like structures. At high pH (Figure 4(b)), the likelihood of strong intermolecular hydrogen-bonding interactions is relatively less due to the deprotonated carboxylate moieties, resulting in smaller architectures forming at high pH due to the repulsion between the carboxylate groups. However, hydrogen-bonding interactions as well as stacking interactions are still observed between the hydroxyl groups leading to the formation of the spherical structures.

To further elucidate the mechanism for the self-assembly of chicoric acid, FT-IR spectroscopy was employed (Figure 5). We compared the spectra of pure chicoric acid with that of self-assembled chicoric acid microtubular networks obtained at pH 4. In the case of pure chicoric acid, we observed peaks at 1728 and 1701 cm^{-1}, which are assigned to the keto-ester groups and the symmetric C═O stretching vibrations due to the carboxylic acid groups, respectively. The peak at 1656 and 1635 cm^{-1} are assigned to the asymmetric C═O stretching mode of the free keto-carbonyl group and the carboxyl groups. The band at 1602 cm^{-1} is assigned to C═C in ring stretching vibration due to the benzene rings. Furthermore, –OH peaks are observed at 3562 and 3502 cm^{-1}. In the case of the self-assembled microtubular structures, we observed red shifts compared to pure chicoric acid. The hydroxyl peaks are red shifted to 3390 and 3323 cm^{-1}. Peaks were observed at 1699, 1670 and 1631 cm^{-1} due to the keto-ester and C═O groups of the carboxylic acid (*49*). Additionally, the peak due to the C═C in ring stretching vibration is red shifted to 1556 cm^{-1} indicating that stacking interactions are also involved in the self-assembly process. The peak due to C═O stretching at 1263 cm^{-1} in the pure chicoric acid is red shifted to 1253 cm^{-1} in the assembled structures. The appearance of these shifts indicates that the formation of higher order species, such as dimers/trimers/oligomers, formed due to inter- and intramolecular hydrogen-bonding interactions.

To determine the effect of pH on the ionic charge and protonation and deprotonation of the microstructures, zeta potential analyses were carried out. As shown in Figure 6, it was observed that as the pH of the samples increased, the zeta potential values decreased. This is most likely because at low pH, the carboxyl groups are protonated. As deprotonation occurs, the zeta potential becomes progressively negative due to the loss of the hydrogens from the carboxyl groups, thus confirming that hydrogen-bonding, as well as electrostatic, interactions play a major role in the formation of the self-assembled architectures. The graph of the zeta potential analysis resembles the titration curve of a diprotic acid, suggesting that the

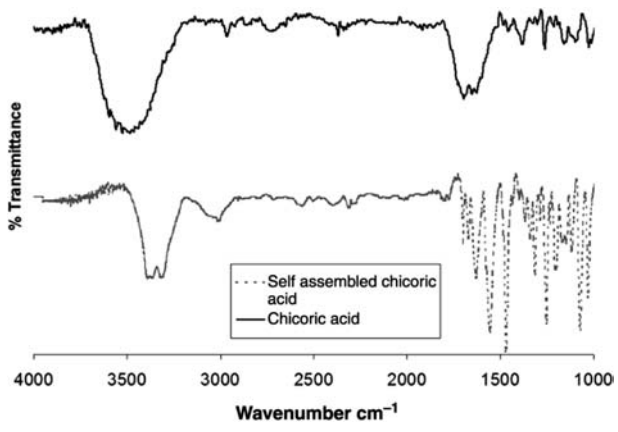

Figure 5. Comparison of FT-IR spectra of self-assembled microtubular assemblies at low pH, with neat chicoric acid.

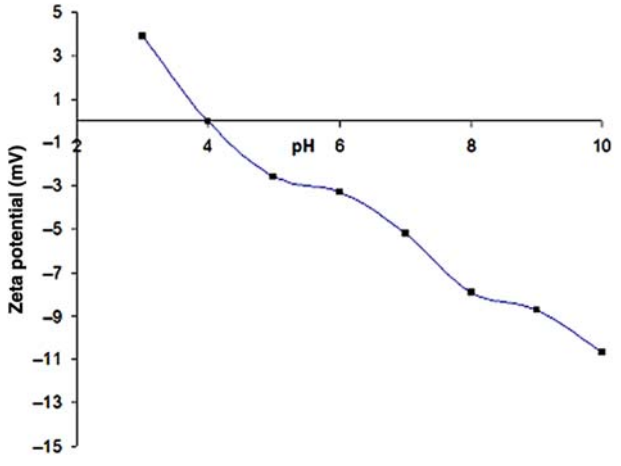

Figure 6. ζ-Potential analysis of self-assembled chicoric acid microstructures.

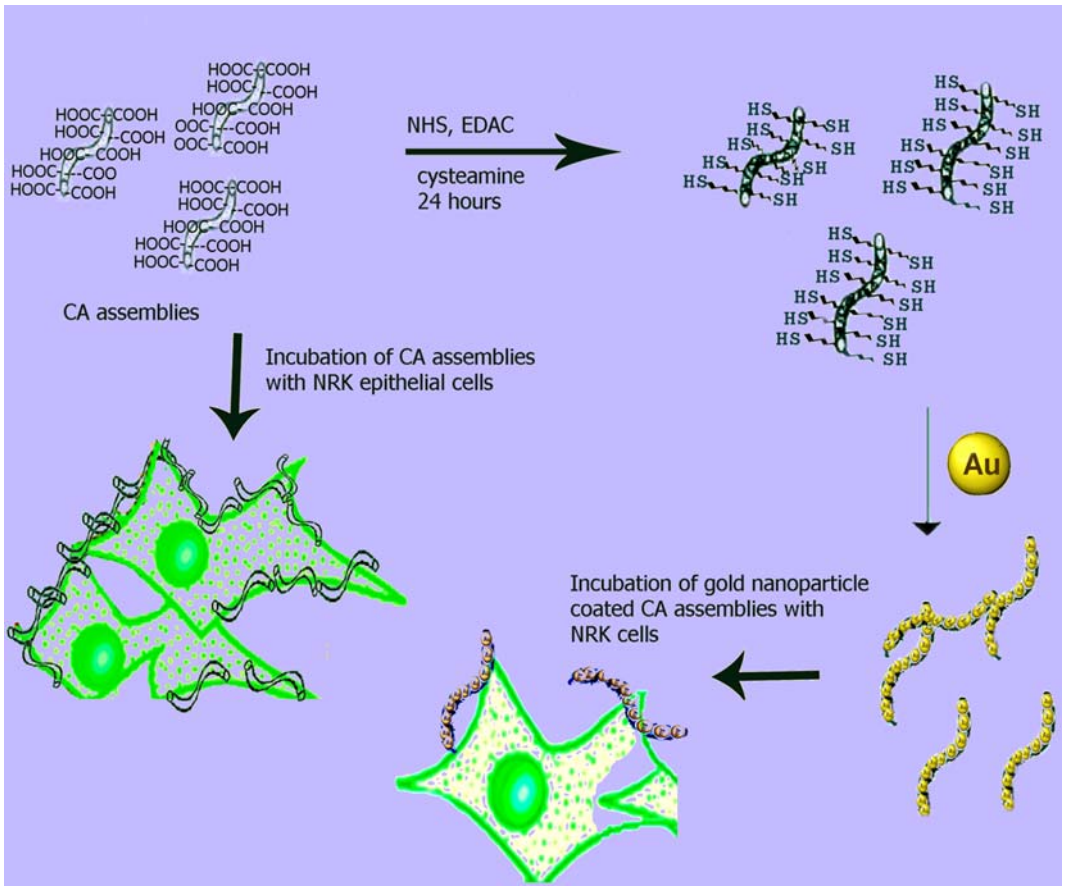

Scheme 1.

—COOH groups of chicoric acid are deprotonated at different pHs, thus allowing for further tailoring of the resultant architectures by optimising the degree of protonation desired.

Conjugation of chicoric acid assemblies with gold nanoparticles

The chicoric acid nanofibrillar structures assembled at a pH range of 3–5 were formed in high yields, and were, therefore, used as templates for the attachment of gold nanoparticles on the surfaces. The scheme for the formation of the gold nanoparticle-coated assemblies and subsequent attachment to NRK epithelial cells is shown in Scheme 1. Because the self-assembled chicoric acid nanofibrillar structures incorporate free carboxylic groups on the surfaces, those groups can be utilised as binding sites to anchor molecules and metal ions to construct various functionalised nanostructures, by simple incubation methods. Furthermore, because these binding sites are distributed on the entire nanofibre surfaces, after functionalisation with cysteamine, gold nanoparticles can be immobilised uniformly on the surface of the nanostructures. Similar functionalisations on nanostructure surfaces have also been carried out using carbon nanotubes and peptide nanotubes (*50*, *51*). Thus, the nanostructures were incubated with the organic linker cysteamine by utilising *N*-hydroxysuccinimide (NHS) and 1-ethyl-3-(3-dimethylaminopropyl)carbodiimide, hydrochloride (EDAC) to covalently couple cysteamine to the carboxyl groups available on the chicoric acid assemblies, which imparts thiol functionality to the assemblies. We then incubated the functionalised assemblies with gold nanoparticles (15–20 nm in diameter), which were previously prepared by the gold-citrate reduction method. After 24 h, the nanostructures were washed and centrifuged to remove any unattached gold nanoparticles on the surfaces of the nanofibres. FT-IR spectroscopy was employed to confirm the attachment of cysteamine, as well as the conjugation with gold nanoparticles. As shown in the supplementary information, a sharp —NH amide I stretching vibration at 1651 cm^{-1} as well as the —SH mercapto stretch was observed at 2344 cm^{-1}, thus verifying the coupling of the terminal amine of cysteamine to the carboxylic groups of the assemblies of chicoric acid.

To confirm the attachment of gold nanoparticles on the surfaces of the chicoric acid assemblies, electron microscopy was utilised. The transmission electron

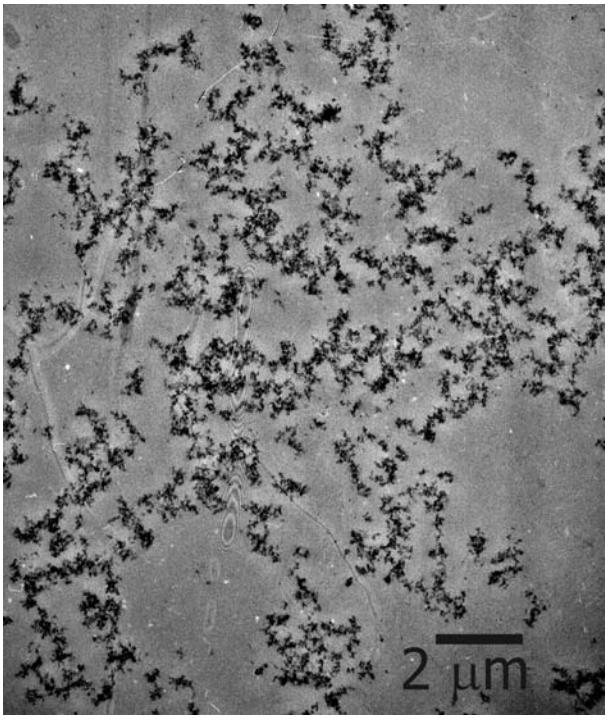

Figure 7. TEM image of gold nanoparticle-coated chicoric assemblies.

microscopy (TEM) image (Figure 7) of the gold nanoparticle-bound assemblies shows the surface of the chicoric acid assemblies coated with gold nanoparticles. The energy dispersive X-Ray (EDX) mapping further confirms the presence of gold nanoparticles on the surfaces of the thiolated chicoric acid assemblies. As can be seen from the structures, the EDX map for gold essentially superimposes the SEM image (Figure 8(a),(b)) obtained for the assemblies, confirming the attachment of gold nanoparticles on the surfaces of the assemblies. The accompanying EDX spectrum (Figure 8(c)) shows the characteristic peaks for gold nanoparticles.

Mammalian cell biocompatability studies

To evaluate the biocompatability of the chicoric assemblies with mammalian cells, samples of bare chicoric acid assemblies or gold nanoparticle-functionalised chicoric acid assemblies were plated with cultured NRK epithelial cells in a cell viability assay. Following incubation for 48 or 72 h, the percent alive cells were determined for each condition (Figure 9). We found that the chicoric acid assemblies and the gold nanoparticles-bound chicoric acid assemblies did not decrease the growth rate and viability of NRK cells by comparison to the solvent (water) controls.

We next wished to determine whether the chicoric acid assemblies could bind to mammalian cells. We, therefore, plated NRK cells with chicoric assemblies as well as the gold nanoparticle-coated chicoric assemblies. Figure 10 shows the NRK cells plated at high (Figure 10(A)) and low (Figure 10(B)) density and cultured for 48 h in the presence of 20 μl of chicoric acid-coated gold nanoparticles. The assemblies attached to the cells and

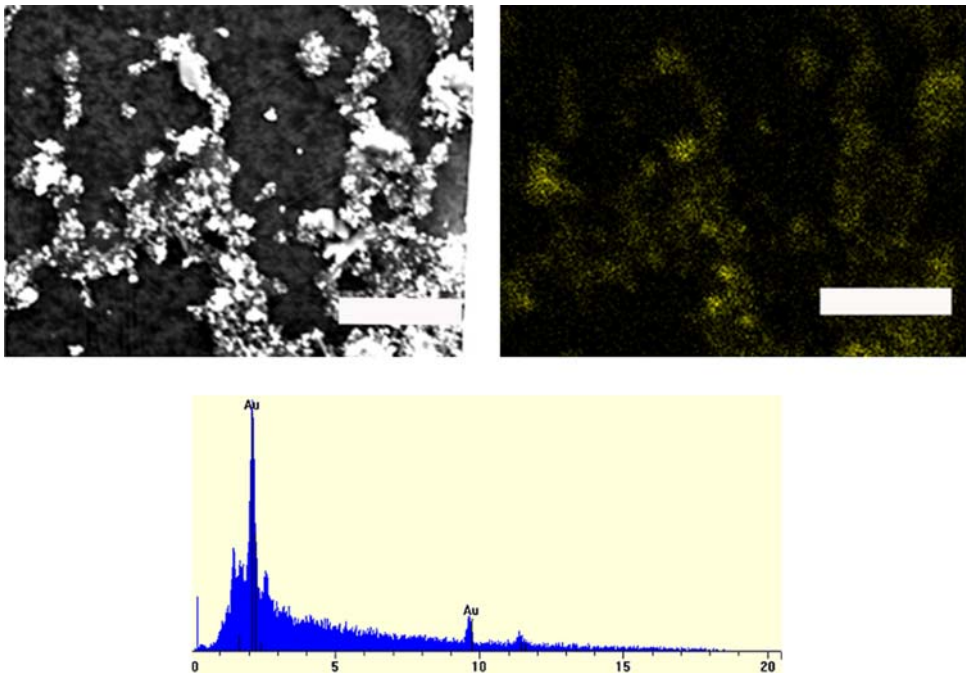

Figure 8. (a) SEM image of chicoric acid assemblies conjugated with gold nanoparticles (scale bar = 5 μm); (b) corresponding EDX map and (c) EDX spectrum.

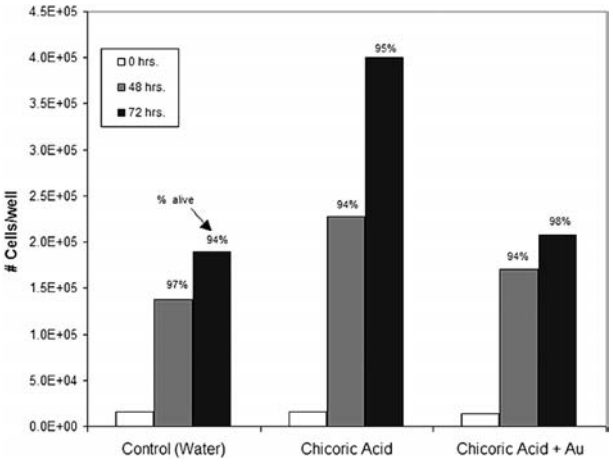

Figure 9. NRK proliferation studies. Cells were incubated with chicoric acid assemblies, gold nanoparticles-coated chicoric acid assemblies or water (solvent control). After 48 and 72 h of incubation, the number of alive cells and the % alive were determined for each condition. This graph shows data from a representative experiment.

several points of attachment of the assemblies are indicated with arrowheads. We did not observe any changes in the morphology of treated cells when compared to control cells cultured at high density for 48 h in the absence of assemblies (Figure 10(C)). Furthermore, we found that the NRK cells and assemblies remained associated when the cells were released from the substrate by trypsinisation to remove cell surface proteins, followed by centrifugation and replating (data not shown). The binding of the uncoated chicoric acid assemblies with NRK cells was also confirmed by electron microscopy (Figure 11). NRK cells were treated with chicoric acid assemblies (Figure 11(B),(C)) or control cells were incubated in complete medium without additions (Figure 11(A)). After 24 h of incubation, the cells were trypsinised, washed to remove unbound assemblies and processed for thin section electron microscopy. We found that the chicoric acid assemblies had attached to the NRK plasma membrane and remained attached during washing and processing for electron microscopy. We found that the assemblies were attached to one side of the trypsin-released cells. This sidedness is consistent with only the upper surface being available when the assemblies were added to adherent cells and suggests that there was neither rearrangement nor post-trypsinisation binding of assemblies during cell processing. More importantly, the morphology of the treated and untreated cells was similar suggesting that the chicoric acid assemblies are biocompatible with NRK cells. Thus, in both cases (with and without gold nanoparticle coating), the chicoric assemblies were found to be not only highly biocompatible, but also adherent to mammalian NRK cells.

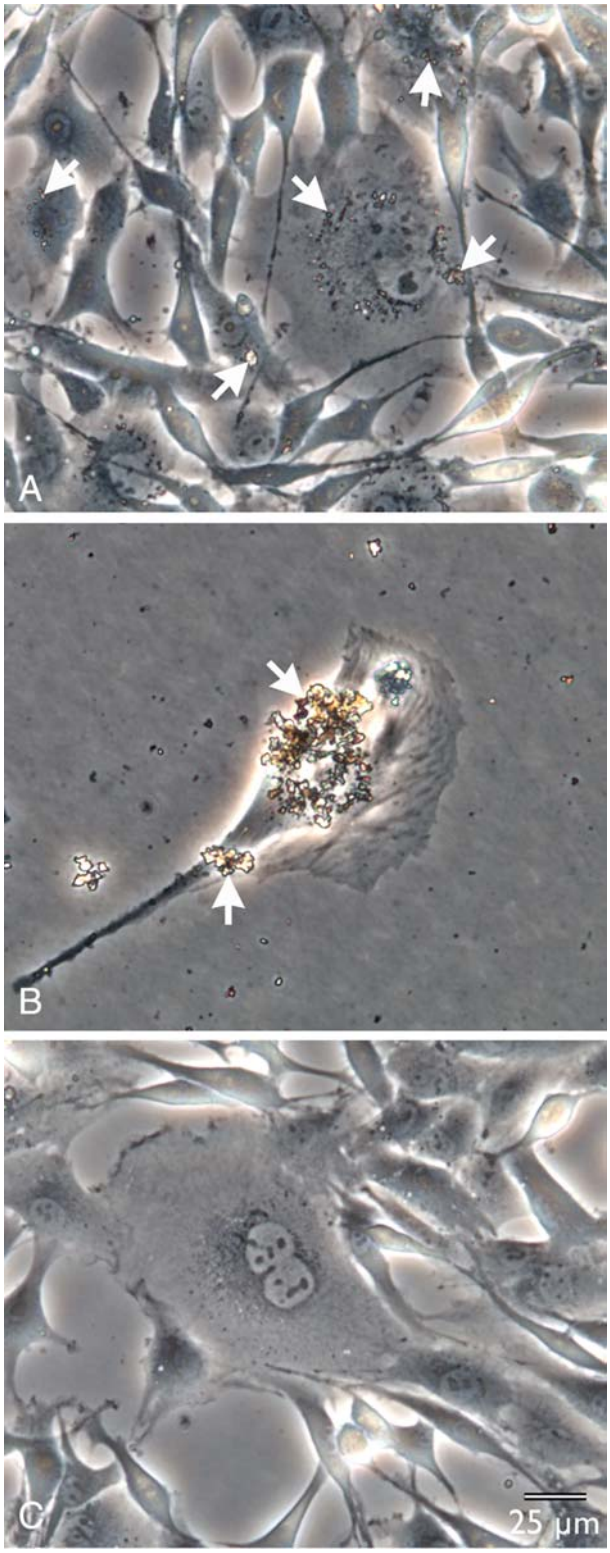

Figure 10. NRK cells plated at high (A) or low (B) density and cultured for 48 h in the presence of 20 μl of chicoric acid-coated gold nanoparticles; (C) control NRK cells cultured at high density for 48 h in the absence of the gold nanoparticle-coated chicoric acid assemblies. (A)–(C) Scale bar = 25 μm.

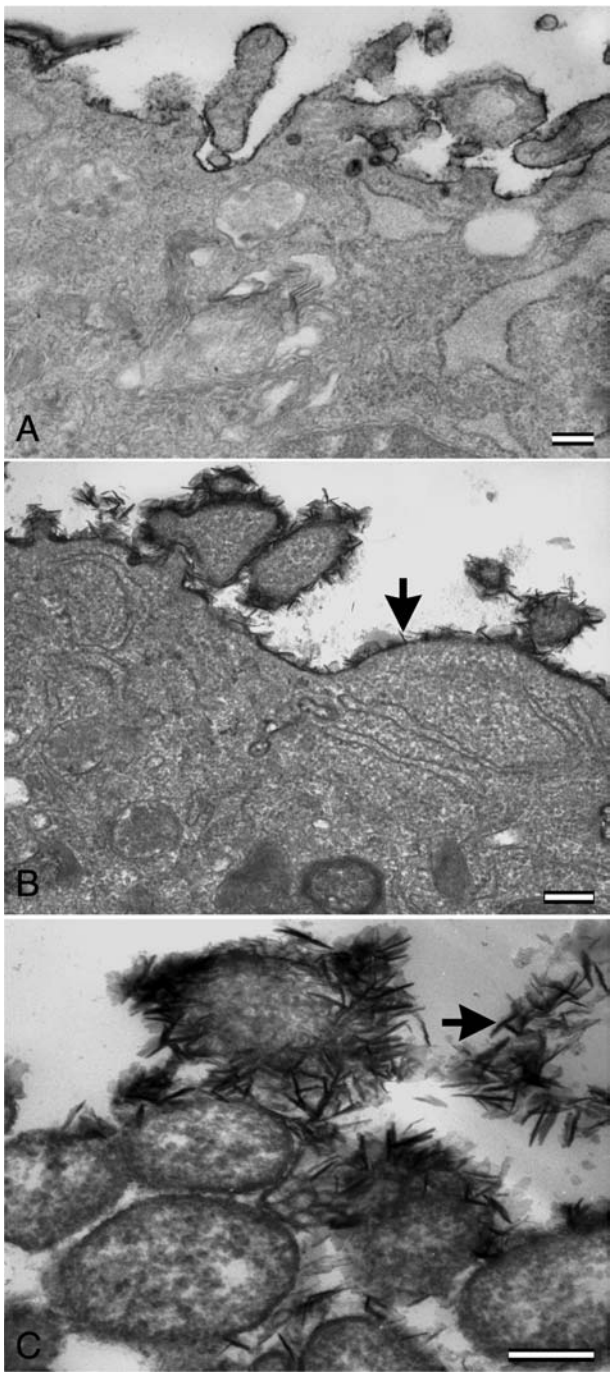

Figure 11. Binding of chicoric acid assemblies to the plasma membrane of NRK cells. (A) NRK cells incubated for 24 h in complete medium (untreated control). (B,C) NRK cells were incubated for 24 h with self-assembled chicoric acid assemblies then released from the tissue culture plate with trypsin. The suspended cells were washed free of trypsin and unbound particles by dilution and low-speed centrifugation before fixation and staining for ultrastructural analysis. The chicoric acid attached and remained bound to the washed NRK cells (arrows in (B) and (C); lower and higher magnification images of different cells), while the plasma membrane of control, untreated cells lacked these assemblies (A). (A)–(C) Scale bar = 200 nm.

Conclusions

In conclusion, chicoric acid was found to form morphologically distinct architectures across a range of pH values. We observed the formation of networks of ribbons, fibres or tubes at low pH and spherical structures at higher pH. The assemblies were then functionalised by coupling cysteamine to the free carboxyl moieties of chicoric acid assemblies by simple incubation method. The uncoated as well as gold nanoparticle-coated chicoric acid assemblies were plated with NRK cells in order to assess the biocompatability of the formed materials, as well as to elucidate the possibility of targeted delivery of chicoric acid into mammalian cell tissues. The morphological and cell growth results suggest strongly that chicoric acid assemblies are biocompatible and non-toxic to mammalian cells. It is likely that such nano- and microstructures may be useful in the construction of microarrays to create a new class of materials for targeting mammalian cells or for the fabrication of devices for sensors and optoelectronics.

Experimental

Materials

Chicoric acid, NHS, EDAC, cysteamine and hydrogen tetrachloroaurate, citric acid were purchased from Sigma-Aldrich. Buffer solutions of varying pH were purchased from Fisher-Scientific. Solutions were used as received.

Self-assembly of chicoric acid nano- and microstructures

Chicoric acid (0.1 M) was allowed to self-assemble at a pH range of 3–10 over a period of 3–4 weeks at room temperature. The samples were shaken slowly for 3 h, and then allowed to sit undisturbed over the entire period of growth. The assemblies obtained were then washed and centrifuged thrice with deionised water before further analysis.

Functionalisation with cysteamine

The assemblies obtained at pH 5 (500 μl, 0.1 mM) were incubated for 24 h with 0.1 mM NHS and 0.1 mM EDAC (200 μl each) in order to activate the carboxyl groups of chicoric acid. The samples were then washed and centrifuged twice at 15,000 rpm before incubation with cysteamine (0.1 M).

Attachment of gold nanoparticles on chicoric acid assemblies

The functionalised thiolated assemblies of chicoric acid were incubated with gold nanoparticle solution (200 μl)

prepared previously by the citrate reduction method (*52*), for a period of 48 h to allow the free sulfhydryl groups of the functionalised assemblies to bind to gold nanoparticles. The samples were washed and centrifuged to remove any unbound gold nanoparticles.

Biocompatibility and cell viability assay

NRK epithelial cells were obtained from the America Type Culture Collection (CRL-6509) and were cultured in Dulbecco's Modified Eagle's Medium (GIBCO) supplemented with 100 units/ml of penicillin, 100 μg/ml of streptomycin, and 10% of foetal bovine serum (complete medium) at 37°C in a humidified atmosphere of 5% CO_2. For morphological analysis, cells were collected using 0.25% Trypsin and 0.1% EDTA in Hank's Balanced Salt Solution (HBSS), and then plated in 2 ml cell culture medium in 12-well Costar plates at low density (2.6×10^4 cells/cm^2) or high density (6.5×10^4 cells/cm^2). After allowing the cells to attach and spread for several hours, 20 μl of chicoric acid-coated gold nanoparticles or water (control solvent) were added to each well and incubated for up to 4 days. To quantify cell proliferation/viability, NRK cells were plated at low density for several hours and then 20 μl of chicoric acid assemblies, chicoric acid-coated gold nanoparticles, or water were added to each well. After 48 or 72 h of growth in the presence of additives, the adherent and any unattached cells were collected from each well by trypsinisation and the number of live and dead cells was determined by trypan blue exclusion.

Molecular modelling studies

Molecular modelling studies were carried out using the program ChemBio 3D ultra, a component of the ChemBioOffice software by taking into account the protonation states of the molecules at varying pH.

Cellular studies using electron microscopy

NRK cells were grown and treated as described for the biocompatibility studies. The cells were then rinsed with HBSS to remove unbound assemblies and serum proteins, and then trypsinised. The released cells were re-suspended with a five- to sixfold dilution into complete cell culture medium to inhibit residual trypsin and then pelleted. The pellets and 1 ml of the supernatant were transferred to centrifuge tubes and the cells repelleted at 240 g for 4 min. The pellets were fixed with 3% glutaraldehyde (Electron Microscopy Sciences, Hatfield, PA, USA), 0.2% tannic acid in 0.1 M $NaPO_4$, pH 7.0 for 60 min at room temperature. The fixed cells were pelleted, re-suspended in phosphate-buffered saline (PBS), and repelleted. The cells were postfixed with 0.5% osmium tetroxide, 0.8% $K_3Fe(CN)_6$ in 0.1 M $NaPO_4$ for 30 min at room temperature in the dark. The osmicated cells were then rinsed once with PBS and once with distilled water. The cells were *en bloc* stained with 2% uranyl acetate in 10% acetone for 5 min and then dehydrated in graded acetones and embedded in Araldite 502 (Electron Microscopy Sciences). Thin sections were stained with aqueous uranyl acetate and lead citrate.

Instrumentation

Scanning electron microscopy was carried out using a Hitachi S-2600N operated at 25 kV. The washed samples were dried and carbon coated before analysis. Transmission electron microscopy was conducted using a JEOL 1200EX microscope. AFM was carried out using a Quesant Universal SPM instrument in tapping mode in air and a silicon–nitride cantilever. Samples were washed twice with distilled water and deposited on the surface of a glass slide and air dried before analysis. FT-IR analyses were carried out using a Matteson Infinity IR equipped with DIGILAB, ExcaliBur HE Series FTS 3100 software. The samples were dried in a vacuum overnight at 30°C and -635 mmHg and mixed with KBr to make pellets for analysis. All spectra were taken at 4 cm^{-1} resolutions with 100 scans taken for averaging. Sample measurements were carried between 400 and 4000 cm^{-1}. Zeta potential analyses were carried using a NICOMP 380 ZLS zeta potential/particle sizer system. Measurements of ζ-potential of the samples were carried out at 25°C and at varying pH. The concentrations of the suspensions were adjusted within the operational limits of the instrument, and the suspension pH was adjusted by the addition of standard buffer solutions. The reported ζ-potential values are the average of at least five measurements (spread of values ± 5% of the reported mean values). To record the association of gold particles with NRK cells, photographs were taken using an inverted Leica DMIC phase microscope with attached Leica DFC 420 digital camera.

Acknowledgements

The authors thank Dr Patrick Brock of the Queens College, CUNY, Department of Geology for the use of the scanning electron microscope. E.S. thanks the Trinity Charitable Fund Award for financial support. K.F. thanks Omid Khalpari and Rivka Lederman for their assistance with ultrastructural analysis. This work was conducted in part using instruments in the Queens College Core Facility for Imaging, Cell and Molecular Biology. These studies were funded by grants from the Fordham University Faculty Research Program (I.B.), PSC–CUNY (K.F.), and the Undergraduate Research/Mentoring Education initiative at Queens College (K.F.).

References

(1) Li, L.-L.; Fang, C.-J.; Sun, H.; Yan, C.-H. *Chem Mater.* **2008**, *20*, 5977–5986.
(2) Miao, X.; Chen, C.; Zhou, J.; Deng, W. *Appl. Surf. Sci.* **2010**, *256*, 4647–4655.
(3) Kato, T. *Supramol. Sci.* **1996**, *3*, 53–59.
(4) Schepartz, A.; McDevitt, J.P. *J. Am. Chem. Soc.* **1989**, *111*, 5976–5977.
(5) Viney, C. *Curr. Opin. Solid State Mater. Sci.* **2004**, *8*, 95–101.
(6) Jin, Y.; Qi, N.; Tong, L.; Chen, D. *Int. J. Pharm.* **2010**, *386*, 268–274.
(7) Zhang, S. *Biotechnol. Adv.* **2002**, *20*, 321–339.
(8) Wu, Z.-Q.; Jiang, X.-K.; Li, Z.-T. *Tetrahedron Lett.* **2005**, *46*, 8067–8070.
(9) Taylor, D.M.; Fukushima, H.; Morgan, H. *Supramol. Sci.* **1995**, *2*, 75–87.
(10) Pallavicini, P.; Diaz-Fernandez, Y.A.; Pasotti, L. *Coord. Chem. Rev.* **2009**, *253*, 2226–2240.
(11) Onoda, M.; Tada, K.; Nakayama, H. *Synth. Met.* **1999**, *102*, 1253.
(12) Huang, C.-H.; McClenaghan, N.D.; Kuhn, A.; Bravic, G.; Bassani, D.M. *Tetrahedron* **2006**, *62*, 2050–2059.
(13) Pereira, G.G. *Curr. Appl. Phys.* **2004**, *4*, 255–258.
(14) (a) Drummond, C.J.; Fong, C. *Curr. Opin. Colloid Interface Sci.* **2000**, *4*, 449–456. (b) Cui, H.; Muraoka, T.; Cheetham, A.G.; Stupp, S.I. *Nano Lett.* **2009**, *9*, 945–951. (c) Kogiso, M.; Ohnishi, S.; Yase, K.; Masuda, M.; Shimizu, T. *Langmuir* **1998**, *14*, 4978–4986.
(15) (a) Vemula, P.K.; Cruikshank, G.A.; Karp, J.M.; John, G. *Biomaterials* **2009**, *30*, 383–393. (b) Hartgerink, J.D.; Granja, J.R.; Milligan, R.A.; Ghadiri, M.R. *J. Am. Chem. Soc.*, **1996**, *118*, 43–50.
(16) Li, H.; Carter, J.D.; LaBean, T.H. *Mater. Today* **2009**, *12*, 24–32.
(17) Tabaei, S.R.; Jönsson, P.; Brändén, M.; Höök, F. *J. Struct. Biol.* **2009**, *168*, 200–206.
(18) Niemeyer, C.M. *Curr. Opin. Chem. Biol.* **2000**, *4*, 600–618.
(19) Yang, Y.; Khoe, U.; Wang, X.; Horii, A.; Yokoi, H.; Zhang, S. *Nano Today* **2009**, *4*, 193–210.
(20) Safinya, C.R. *Curr. Opin. Struct. Biol.* **2001**, *11*, 440–448.
(21) Fameau, A.-L.; Houinsou-Houssou, B.; Novales, B.; Navailles, L.; Nallet, F.; Douliez, J.-P. *J. Colloid Interface Sci.* **2010**, *341*, 38–47.
(22) Huang, P.-H.; Lin, J.T.; Yeh, M.-C.P. *J. Organomet. Chem.* **2006**, *691*, 975–982.
(23) Yan, D.; Zhou, Y.; Hou, J. *Science* **2004**, *303*, 65–67.
(24) (a) Xu, C.; Kopečk, J. *Polym. Bull.* **2007**, *58*, 53–63. (b) Jayawarna, V.; Ali, M.; Jowitt, T.A.; Miller, A.F.; Saini, A.; Gough, J.E.; Ulijin, R.V. *Adv. Mater.* **2006**, *18*, 611–614.
(25) Liu, T. *J. Am. Chem. Soc.* **2003**, *125*, 312–313.
(26) Šilhar, P.; Čapková, K.; Salzameda, N.T.; Barbieri, J.T.; Hixon, M.S.; Janda, K.D. *J. Am. Chem. Soc.* **2010**, *132*, 2868–2869.
(27) Cos, P.; Maes, L.; Berghe, D.V.; Hermans, N.; Pieters, L.; Vlietinck, A. *J. Nat. Prod.* **2004**, *67*, 284–293.
(28) Smoak, E.M.; Carlo, A.D.; Fowles, C.C.; Banerjee, I.A. *Nanotechnology* **2010**, *21*, 25603–25612.
(29) (a) Sembdner, G.; Borgmann, E.; Schneider, G.; Liebisch, H.W.; Miersch, O.; Adam, G.; Lischewski, M.; Schrefber, K. *Planta* **1976,** *132*, 249–257. (b) Weiler, E.W.; Wieczorek, U. *Planta* **1981**, *152*, 159–167.
(30) Fowles, C.C.; Smoak, E.M.; Banerjee, I.A. Colloids Surf. *B* **2010**, *78*, 250–258.
(31) Long, Y.Q.; Jiang, X.-H.; Dayam, R.; Sanchez, T.; Shoemaker, R.; Sei, S.; Neamati, N. *J. Med. Chem.* **2004**, *47*, 2561–2573.
(32) Wei, D.; Sun, W.; Qian, W.; Ye, Y.; Ma, X. *Carbohydr. Res.* **2009**, *344*, 2375–2382.
(33) Huo, Q. *Colloid Surf. B* **2007**, *59*, 1–10.
(34) Lee, J.; Scagel, C.F. *Food Chem.* **2009**, *115*, 650–656.
(35) Pan, M.; Guo, X.; Cai, Q.; Li, G.; Chen, Y. *Sens Actuat. A* **2003**, *108*, 258–262.
(36) Thakkar, K.N.; Mhatre, S.S.; Parikh, R.Y. *Nanomed: NBM* **2010**, *6*, 257–262.
(37) Mandal, S.; Phadtare, S.; Sastry, M. *Curr. Appl. Phys.* **2005**, *5*, 118–127.
(38) Su, J.; Tao, X.; Xu, H.; Chen, J.-F. *Polymers* **2007**, *48*, 7598–7603.
(39) Jokerst, J.V.; Raamanathan, A.; Christodoulides, N.; Floriano, P.N.; Pollard, A.A.; Simmons, G.W.; Wong, J.; Gage, C.; Furmaga, W.B.; Redding, S.W.; McDevitt, J.T. *Biosens. Bioelectron.* **2009**, *24*, 3622–3629.
(40) Yap, F.L.; Zhang, Y. *Biosens. Bioelectron.* **2007**, *22*, 775–788.
(41) Tallury, P.; Malhotra, A.; Byrne, L.M.; Santra, S. *Adv. Drug Delivery Rev.* **2010**, *62*, 424–437.
(42) Du, D.; Ding, J.; Cai, J.; Zhang, A. *Sens. Actuat. B* **2007**, *127*, 317–322.
(43) (a) Yan, X.; Cui, Y.; He, Q.; Wang, K.; Li, J. *Chem. Mater.* **2008**, *20*, 1522–1526. (b) Bhat, S.; Maitra, U. *Chem. Mater.* **2006**, *18*, 4224–4226. (c) Kimura, M; Kobayashi, S.; Kuroda, T.; Hanabusa, K.; Shirai, H. *Adv. Mater.* **2004**, *16* (4), 335–338. (d) Bose, P.P.; Drew, M.G.B.; Banerjee, A. *Org. Lett.* **2007**, *9* (13), 2489–2492. (e) van Herrikhuyzen, J.; George, S.J.; Vos Matthijin, R.J.; Sommerdijk, N.A.J.M.; Ajayaghosh, A.; Meskers, S.C.J.; Schenning, A.P.H.J. *Angew. Chem., Int. Ed.* **2007**, *46*, 1825–1828. (f) Bhattacharya, S.; Srivastava, A.; Pal, A. *Angew. Chem., Int. Ed.* **2006**, *45* (18), 2934–2937. (g) Basit, Hajra, Pal, A.; Sen, S., Bhattacharya, S. *Chem. Eur. J.* **2008**, *14*, 6534–6545. (h) Bose, P.P.; Drew, M.G.B.; Das, A.K.; Banerjee, A. *Chem. Commun.* **2006**, *30*, 3196–3198. (i) Ray, S., Das, A.K., Banerjee, A. *Chem. Commun.* **2006**, *26*, 2816–2818. (j) Mantion, A., Guex, A.G., Foelske, A., Mirolo, L., Fromm, K.M., Painsi, M., Taubert, A. *Soft Matter.* **2008**, *4* (3), 606–617. (k) Coates, I.A., Smith, D.K.J. *Mater. Chem.* **2010**, *20*, 6696–6702.
(44) (a) Lin, Z.; Neamati, N.; Zhao, H.; Kiryu, Y.; Turpin, J.A.; Aberham, C.; Strebel, K.; Kohn, K.; Witvrouw, M.; Pannecouque, C.; Debyser, Z.; De Clercq, E.; Rice, W.G.; Pommier, Y.; Burke, Jr., T.R. *J. Med. Chem.* **1999**, *42*, 1401–1414. (b) Di Santo, R.; Costi, R.; Rouxm, A.; Miele, G.; Crucitti, G.C.; Iacovo, A.; Rosi, F.; Lavecchia, A.; Marinelli, L.; Di Giovanni, C.; Novellino, E.; Palmisano, L.; Andreotti, M.; Amici, R.; Galluzzo. C.M.; Nencioni, L.; Palamara, A.T.; Pommier, Y.; Marchand, C. *J. Med. Chem.* **2008**, *51*, 4744–4750.
(45) Robinson, W.E.; Cordeiro, M.; Abdel-Malek, S.; Jia, Q.; Chow, S.A.; Reinecke, M.G.; Mitchell, W.M. *Mol. Pharmacol.* **1996**, *50*, 846–855.
(46) (a) Gazit, E. *Chem. Soc. Rev.* **2007**, *36*, 1263–1269. (b) Gao, X.; Matsui, H. *Adv. Mater.* **2005**, *17*, 2037–2050. (c) Kinge, S.S.; Crego-Calama, M.; Reinhoudt, D.N. *Langmuir* **2007**, *23*, 8772–8777.
(47) (a) Xia, Y.; Rogers, J.A.; Paul, K.E.; Whitesides, G.M. *Chem. Rev.* **1999**, *99*, 1823–1848. (b) Maura, R.; Yoshida, K.; Masuda, M.; Yase, K.; Shimizu, T. *Chem. Mater.* **2002**, *14*, 3047.

(48) Thurman, E.M. *Organic Geochemistry of Natural Water*; Kluwer Academic Publishers: Dordrecht, 1985.
(49) (a) Dong, J.; Tsubahara, N.; Fujimoto, Y.; Ozaki, K.; Nakashima, *Appl. Spectroscopy* **2001**, *55*, 1603–1609. (b) Stefan, I. C.; Mandler, D.; Scherson, D. A. *Langmuir* **2002**, *18*, 6976–6980.
(50) Banerjee, I.A.; Yu, L.; Matsui, H. *Nano Lett.* **2003**, *3*, 283–287.
(51) (a) Kim, B.; Sigmund, W. M. *Langmuir* **2004**, *20*, 8239–2842. (b) Banerjee, I. A.; Yu, L.; MacCuspie, R. I.; Matsui, H. *Nano Lett.* **2004**, *4*, 2437–2440.
(52) Turkevich, J.; Stevenson, P.C.; Hillier *J. Discuss. Faraday Soc.* **1951**, *11*, 55–75.